Optical fibers for miniaturized surface-enhanced Raman-scattering probes

Jennifer S. Hartley,[1,*] Saulius Juodkazis,[2] and Paul R. Stoddart[1]

[1]Centre for Atom Optics and Ultrafast Spectroscopy, Faculty of Engineering and Industrial Sciences, Swinburne University of Technology, Hawthorn, Victoria 3122, Australia

[2]Centre for Micro-Photonics and Melbourne Centre for Nanofabrication, Faculty of Engineering and Industrial Sciences, Swinburne University of Technology, Hawthorn, Victoria 3122, Australia

*Corresponding author: jhartley@swin.edu.au

Received 17 September 2013; revised 5 November 2013; accepted 7 November 2013; posted 8 November 2013 (Doc. ID 197865); published 25 November 2013

A range of optical fibers with surface-enhanced Raman scattering (SERS) functionalized tips have been evaluated for use as micro-scale sensing devices. In order to optimize the sensitivity of the optical fiber probe, the relationship between SERS intensity and different fiber parameters was investigated. It was found that the numerical aperture, core size, mode structure, and core material have a major effect on the probe performance, as does the numerical aperture of the microscope objective. The results suggest that an ideal fiber for SERS sensing should be single mode at the excitation wavelength and have low-background core material. © 2013 Optical Society of America

OCIS codes: (060.2270) Fiber characterization; (060.2370) Fiber optics sensors; (160.2290) Fiber materials; (170.5660) Raman spectroscopy; (240.6695) Surface-enhanced Raman scattering; (300.6450) Spectroscopy, Raman.

http://dx.doi.org/10.1364/AO.52.008388

1. Introduction

Optical fibers are attractive for use in Raman spectroscopic probes due to their remote-sensing capability, thermal and chemical passivity, and compact size [1]. In general, the use of optical fibers probes in Raman spectroscopy can be categorized as "extrinsic" or "intrinsic" [2]. Where the fiber is simply used to link the spectroscopic instrumentation to the sampling point, it is referred to as an extrinsic probe. In intrinsic probes, the waveguide itself plays a role in the measurement process. For example, hollow waveguides can be used for the measurement of gaseous or liquid analytes, with long path lengths being possible if the analyte solution has a higher refractive index than the hollow-fiber material [2,3].

Intrinsic sensing approaches are attractive for surface-enhanced Raman scattering (SERS), where a nanostructured metal surface is required to generate the enhanced scattering signal. The SERS substrate can either be drawn into the core of a hollow fiber [4,5] or the air channels of solid core photonic crystal fiber [6,7], or alternatively, it can be deposited directly onto the end-face of a solid core fiber [1,8,9] in an optrode configuration. In all of these approaches, a single fiber can be used for excitation and collection from the analyte. However, conventional solid core/clad fibers may offer greater generality of application, as they do not require the sample to be drawn into the structure of the fiber.

These different modes of sensing have a major bearing on the potential for miniaturizing Raman probes. Normal Raman scattering is a relatively weak effect that scales with the sample volume. This favors high-throughput probes based on large-core, high-NA fibers. However, these fibers generate

1559-128X/13/348388-06$15.00/0

additional Raman background, which may swamp the signal if it is not removed by bulk optical filters. Consequently, the smallest reported extrinsic Raman probe has a diameter of 600 μm [10]. Recent work has shown that the filters can be removed by using a hollow-core photonic-crystal fiber to deliver the excitation with reduced background [11], while fiber Bragg gratings can be used in the collection fibers to remove the Rayleigh scattering [12]. In this way, the probe diameter could in principle be reduced to less than 400 μm.

In contrast to normal Raman, SERS can provide significant signal amplification (on the order of 10^6 to 10^8) for analyte molecules adsorbed on a SERS-active metal surface. When combined with the single-ended optrode sensing approach, the size of intrinsic SERS probes potentially could be significantly reduced. Indeed, the potential for miniaturization has been demonstrated by the recent progress in tip-enhanced Raman scattering (TERS) [13]. However, TERS generally relies on high NA microscope objectives to collect externally scattered light and remains a highly specialized technique that is best suited to applications requiring high spatial resolution. Thus there remains a need for robust and alignment-free miniaturized SERS probes in a broad range of chemical and biological trace-sensing applications [14]. Miniaturized SERS probes have particular potential for biomedical applications, including remote testing for cancer [15] or for minimally invasive continuous glucose measurements [16].

Despite these important potential applications, there have been relatively few studies on the optimal characteristics of optical fibers for SERS optrodes. The relationship between SERS intensity and fiber NA, core size, and material must be optimized to achieve the best sensing performance. The importance of matching the source area and solid angle (etendue) to the spectrometer entrance slit has been appreciated for extrinsic Raman probes [17]. Recent work on the collection efficiency of an intrinsic SERS probe based on multimode telecommunication fiber has suggested that the numerical aperture (NA) of a fiber should be matched to the NA of the excitation/collection objective, while the fiber core size should match the projection of the spectrometer slit onto the fiber [18]. The throughput of the combined optical fiber-spectrometer system can be described by

$$\frac{I_{\mathrm{fib}}}{I_{\mathrm{dir}}} \propto \left(\frac{\Omega_{\mathrm{fib}}}{\Omega_{\mathrm{obj}}}\right)\left(\frac{\rho}{a}\right)^2 \int_0^{\infty} g(z)\mathrm{d}z, \qquad (1)$$

where I_{fib} is the intensity of the scattered light collected through the optical fiber, I_{dir} is the intensity collected directly from the SERS substrate, with both quantities normalized against the respective excitation powers at the SERS substrate, Ω is the solid angle of the fiber/objective, ρ is the radius of the spectrometer entrance pinhole projected onto the fiber core of radius a (the source), and the integral of $g(z)dz$ is the signal contribution from out-of-focus rays [18]. In principle, this ratio can exceed unity due to the additional enhancement that arises in reverse excitation due to the Fresnel mechanism [19]. In previous studies of extrinsic probes [10,20,21], the spectrometer slit was made sufficiently large enough that the fiber core projection was not restricted. However, these large slit sizes may reduce the resolution of the spectrometer and are not indicative of the slits used in practical applications.

From the preceding discussion, there is a lack of reliable data regarding fiber selection for miniaturized SERS optrodes. Therefore, this paper explores the SERS collection efficiency of silica-based fibers with core sizes ranging from 3.0 to 62.5 μm. Although it is known that silica fibers tend to produce less background than other fiber materials, this hasn't been systematically tested for smaller core fibers in the SERS optrode configuration [8,10]. Therefore, a comparison of low- and high-doped fibers will be presented. Furthermore, to investigate the relationship between core size and fiber Raman background, this work used a slit width that is relevant to practical applications (i.e., corresponding to 1 cm^{-1} spectral resolution). This allows fibers that have a range of different NAs to be characterized with a range of microscope objectives in order to confirm the effects of fiber NA and core size on SERS probe performance.

2. Materials and Methods

A. Fiber Probe Design

The single-ended optrode approach does not allow the fiber Raman background to be filtered out. Therefore short fiber lengths of about 25 mm were used in this study to minimize the background. These short lengths are of interest for transcutaneous biosensing. The specifications of the fibers used are listed in Table 1, based on the manufacturer's specifications where available or data on the spool. The V numbers at 514 nm were calculated from the NA and core diameter [22]. The core doping was confirmed by energy-dispersive spectroscopy, performed on a FEI Quanta 200. Each of the test fibers shown in Table 1

Table 1. List of Fiber Types Tested[a]

Fiber ID	NA	Solid Angle (sr)	Core Diameter (μm)	V Number (at 514 nm)	Core Doping
SMF28	0.14	0.061	8.2	7.0	Low GeO_2
MMF	0.272	0.231	62.5	103.8	High GeO_2
SM1500	0.30	0.281	4.2	7.7	High GeO_2
S405	0.12	0.045	3.0	2.2	Pure SiO_2

[a]Cladding diameter of all fibers was 125 μm.

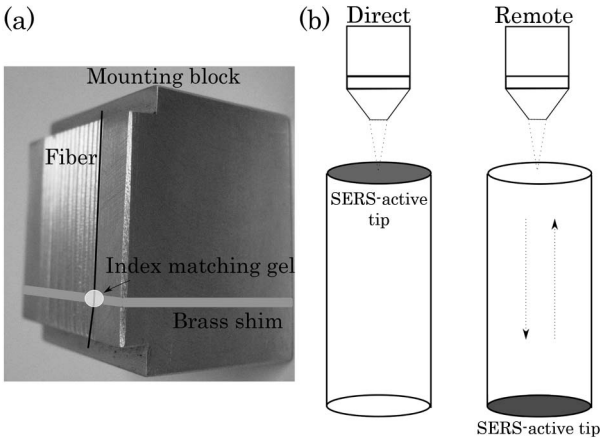

Fig. 1. (a) Samples and mounting block, showing the brass shim used to bend the fibers. (b) Direct and remote-sensing configurations.

were stripped of their jacket and then cleaved at both ends to the required length. A cube of aluminum, 23 mm high, was heated on a hot plate. A thermoplastic adhesive (Crystalbond, 509) was melted across the width of the block, and the fibers were carefully mounted, ensuring that 1 mm of fiber protruded from the block at both ends, as shown in Fig. 1.

For fiber lengths shorter than approximately 1 m, cladding modes are not adequately suppressed and can cause significant uncertainty in terms of coupling efficiency. Therefore index-matching gel (Thorlabs, G608N, $n_D = 1.4646$ at 25°C) was placed along the length of the fiber to remove the cladding modes. However, this was not successful in stripping all of the cladding modes, as the index-matching gel does not exactly match the refractive index at the SERS excitation wavelength (514 nm). A thin sheet of metal (brass shim, 0.2 mm thickness) was slipped underneath the coated end of the fibers, providing an angle larger than the critical angle in order to suppress total internal reflection in the cladding. The required bend angle was determined by inspection of the transmitted light patterns. These efforts ensured that the substrate was uniformly excited and allowed reliable comparison of different fiber types.

B. SERS Substrate Fabrication

A 2 nm chromium adhesion layer was sputtered directly onto the fiber tips. Then silver island films were deposited using the oblique angle deposition technique [9]. This involved 100 nm of silver (Sigma Aldrich, >99.99% 1–3 mm shots) evaporated at an angle of 86° to the surface normal of the fiber tip. The film thickness was measured at normal incidence on a quartz crystal monitor in an Emitech K975X Turbo Evaporator. Note that this substrate fabrication process was chosen to ensure good repeatability between samples, rather than to achieve the highest possible SERS signal. Previous work has demonstrated a repeatability of better than 10% (relative standard deviation) for these metal island films and shown that increased signal levels can be obtained in thicker nanorod films [9]. A number of more highly enhancing substrates are available for future development of the probes [23,24,25,26].

After the film was deposited, the fiber tips were placed in a 10 mM thiophenol (Sigma Aldrich, >99%) solution in ethanol (Sigma Aldrich, 200 proof, anhydrous, >99.5%) for 10 min, rinsed in ethanol for 10 min, and then left to dry in the fume hood for 1 h. Thiophenol is known to form stable and reproducible self-assembled monolayers on silver [8,9].

C. Experimental Setup

A Renishaw inVia Raman Microscope was used for coupling, NA testing, and collecting SERS spectra of the test analyte. The stage has a hollow section where a microscope slide can be mounted. The block (Fig. 1) was carefully placed on the slide, allowing the fibers to protrude off the edge. When the laser was coupled, the transmitted light pattern could be observed underneath the stage.

The spectrometer was operated with an excitation wavelength of 514.5 nm, a holographic notch filter, and a 2400 l/mm grating. The slit width was set to 65 μm, which is a relatively relaxed setting compared to the confocal setting of 20 μm. A range of microscope objectives were used to couple into the fiber. The magnification/NA/solid angles of the objectives were 5 × /0.12/0.04, 10 × /0.25/0.20, 20 × L/0.40/0.52, and 50 × L/0.50/0.84. Spectra were acquired for three accumulations of 10 s. All spectral data has been normalized for excitation power at the SERS substrate and exposure time. For the remote measurements, the excitation power was inferred from measurements of the power transmitted through uncoated fibers. Preliminary testing confirmed that a high level of coupling repeatability could be obtained in both SERS-active and uncoated fibers, based on visual inspection of the transmitted mode pattern (also see Section 3.A). Laser powers in the range 1–5 mW were used, depending on the particular objective and fiber background signal levels.

3. Results and Discussion

A. Elimination of Cladding Modes

The coupled pattern for each fiber was investigated before and after applying index-matching gel and introducing a bend greater than the critical angle. Some examples of the results are shown in Fig. 2. In general there was significant improvement in mode pattern after mode stripping, and in most cases the cladding modes completely disappear. The improvement was particularly significant for the small core fibers (SM1500, S405), but there was not a noticeable difference in the coupling pattern for the multimode fiber (MMF62.5).

B. Fiber Probe Performance

The spectra that exhibited the largest SERS signal are shown for each fiber in Fig. 3. The SERS signal

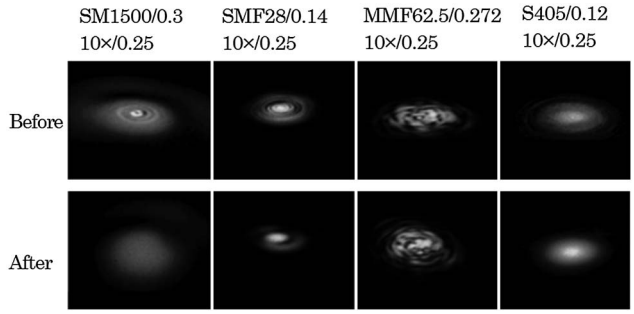

Fig. 2. Examples of projected mode patterns before and after stripping the cladding modes for different fiber/NA, objective/NA combinations. The patterns appear oval as the camera was positioned obliquely due to space constraints. The typical diameter of the pattern on the screen was approximately 2 cm.

was quantified by taking the average intensity of the four major thiophenol peaks at 998, 1022, 1070, and 1572 cm^{-1} (indicated by the dashed lines in Fig. 3). Although different SERS peaks may in general be subjected to different levels of enhancement, no significant changes were observed in the relative peak heights under the conditions of these experiments. This observation is in keeping with previously reported SERS studies of metal-bound thiophenol [25]. Thus the average intensity value is regarded as a satisfactory measure of the overall substrate performance. The fiber Raman background was quantified by taking the peak intensity of the broad silica peak at about 430 cm^{-1} (arrows in Fig. 3). Insets with a magnified intensity scale have been used to highlight the thiophenol peaks for each fiber. The magnified scale also highlights the fiber background in this range, including some additional peaks (e.g., 1156 cm^{-1} in SMF28 and 1590 cm^{-1} in S405) that have been attributed to the core dopants.

In order to compare the basic performance of each fiber as a probe, the average intensity of the remote SERS signal is plotted as a function of the solid angle in Fig. 4. SM1500 delivers the largest signal and shows that the intensity increases as a function of the solid angle. According to Eq. (1), the signal would generally be expected to become constant once the objective collection angle is larger than that of the fiber. However, it is known that the mode structure can take up to 50 m to stabilize [22], so it appears likely that the effective NA of these short fiber sections is higher than suggested by the specifications in Table 1.

The other fibers exhibit a more complex relationship, with the SERS signal peaking at intermediate collection apertures before dropping slightly for the largest collection angle studied here. MMF62.5 provides the lowest signal level for the largest collection angle. This can be understood in terms of factor $(\rho/\alpha)^2$ in Eq. (1), since MMF62.5 has the largest core size of all of the fibers considered here. The size of the entrance slit projected onto the fiber core is smallest for the highest magnitude microscope objective, which corresponds to the largest solid angle. In contrast, the small core fibers are mainly influenced by NA matching.

Perhaps the most important feature of a probe is to have a high ratio of SERS signal to fiber Raman background. This is indicative of the background noise level that the fiber introduces to the SERS signal. SMF28, as seen in Fig. 5, has the highest ratio and therefore the best overall performance of the four fibers. This good performance of SMF28 is largely

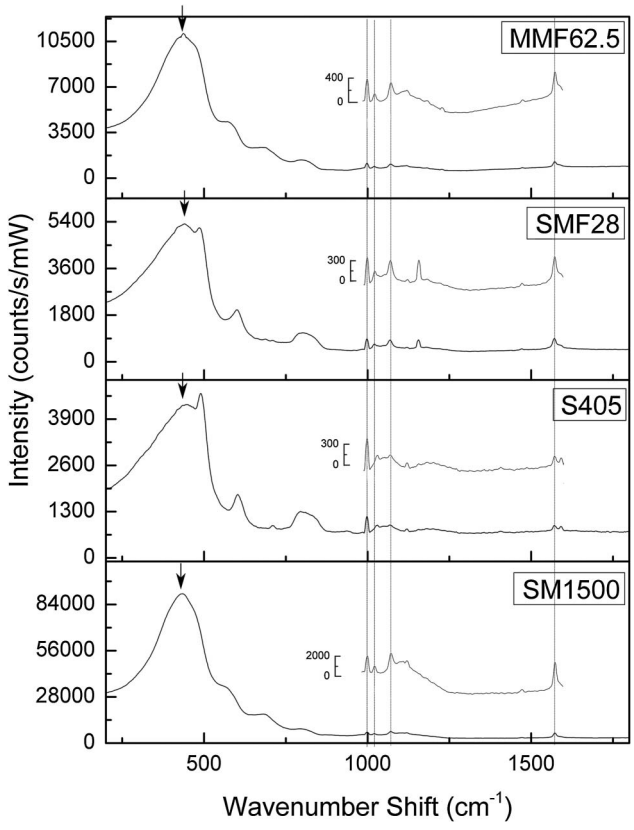

Fig. 3. Comparison of remote measurements for the four fibers. The dashed lines show the main thiophenol SERS peaks, and the arrows show the most intense silica band. These peaks were used to quantify probe performance.

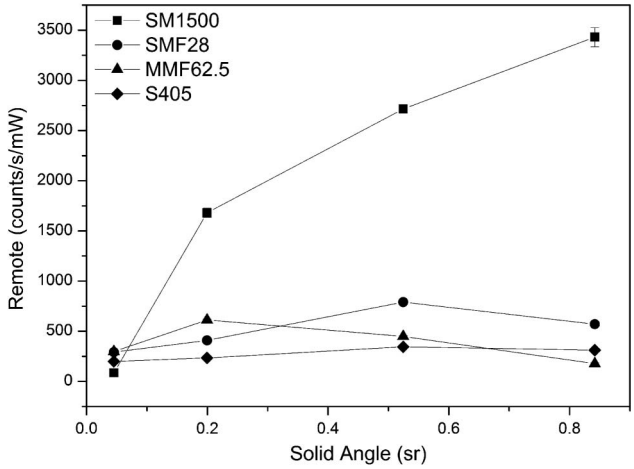

Fig. 4. Average intensity of the thiophenol SERS signal measured in the remote configuration.

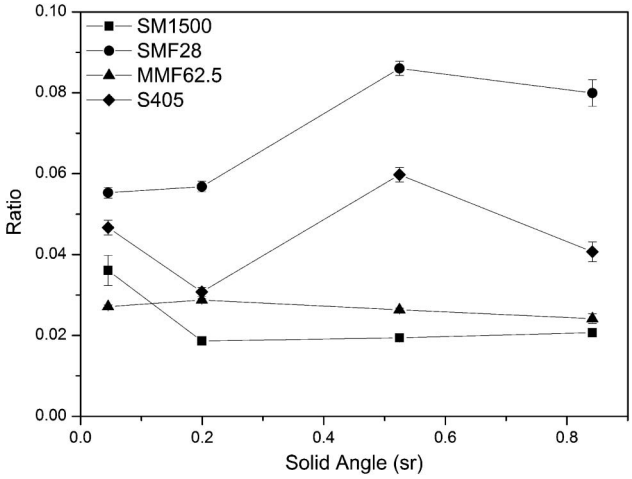

Fig. 5. Ratio of SERS signal to fiber Raman background.

due to the relatively low intensity of the glass Raman spectrum, while the intensity of the SERS signal is comparatively constant (Fig. 4). It has previously been reported that high NA fibers capture more of the Raman scattering generated within the core [20]. However, the high NA fibers also should capture more SERS signal from the tip, leading to no net disadvantage. Therefore the increased background of the high NA fibers may be due to increased levels of Raman scattering from the more highly doped cores. This explanation is indirectly supported by the fact that the glass spectra of the high NA fibers (MMF62.5 and SM1500) are quite different to that of SMF28 and S405 (Fig. 3), which are themselves similar to pure SiO_2 [27]. It should be noted that the fiber background is highly fiber dependent. Motz *et al.* [17] reported that low NA fibers exhibited a high fiber background due to the doping in the cladding.

The ratio of remote to direct SERS (Fig. 6) gives an indication of how much signal is lost or gained when performing a remote measurement through the fiber, as opposed to a direct measurement from the SERS substrate. With close NA matching, each fiber delivers a higher signal in the remote situation than in the direct geometry. This phenomenon recently has been explained in terms of an additional enhancement for the near-field amplitudes that occur due to Fresnel reflection and transmission at the interface [19]. This is certainly the case with SMF28 (low NA fiber) where there is poor NA matching at high objective NA. However, with SM1500, the ratio remains around 1 due to a smaller mismatch with the high NA objectives. SM1500 has the highest capture efficiency and encouragingly SMF28 (highest signal-to-noise ratio) has an efficiency of approximately 1.5 at the lowest collection angle. S405 follows the same trend as SMF28, although it has slightly lower remote intensities (Fig. 4). Once again, MMF62.5 performs poorly at high collection angles due to a poor matching of the source and slit areas, in keeping with Eq. (1) and previous results [18].

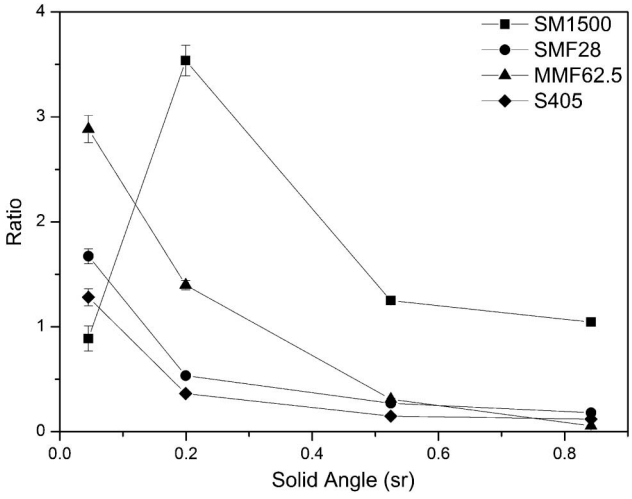

Fig. 6. Ratio of remote to direct SERS intensities.

4. Conclusion

These results suggest that lower dopant levels produce a higher signal-to-background-noise ratio in the remote probe geometry. This implies that pure silica core fibers may be attractive for use as SERS probes. Also, it has been shown that matching the nominal NA of the optical fiber with the NA of the microscope objective is generally not a critical requirement to produce the highest level of SERS signal. This is believed to be due to the presence of leaky modes in these short lengths of fiber. Nevertheless, the highest overall intensities were obtained in the fiber with the highest NA. Further analysis of the fiber-length dependence of the NA will be considered in terms of the beam propagation formalism in future work [28]. Note that a strong dependence on NA would still be expected for longer fibers where the mode structure has stabilized, although the dependence would be expected to match the predictions of Eq. (1) more closely.

Taking all of these factors into consideration, the ideal optical fiber for use in miniaturized SERS probes should offer the following features: low dopant concentration in the core; high NA; and small core size.

To our knowledge, there is no fiber design with all of these ideal characteristics currently available on the market. Of the fibers studied here, SMF28 appears to offer the best combination of properties, but other small core fibers also should be investigated. Note that the development of customized fibers for SERS probes would allow further miniaturization by reducing the fiber cladding diameter from the 125 μm fibers used in this work. We note that silica fibers can also be tapered by acid etching in order to reduce the probe tip diameter down to the size of the core [29].

In terms of core size, single-mode fibers should provide more reproducible performance than few-mode designs because of the stability of the fundamental mode. However, the fibers presented here all displayed similar levels of reproducibility, which suggests that the mode structure may not be a critical

issue if the signal is normalized against the coupled excitation power. If a single-mode fiber is selected, it should be single mode at the excitation and scattering wavelengths to ensure good coupling between the two intensity distributions. While it is generally more difficult to couple light into small cores than large cores, high-precision connectors have allowed widespread use of single-mode fibers (primarily SMF28) in the telecommunications industry.

Previous work has shown that fiber Raman background can also be obtained from hollow core fibers [11]. Although this provides an obvious means to reduce fiber Raman background, the distal end of the fiber would have to be sealed for *in vivo* and *in vitro* studies, adding to the complexity of the construction. Therefore further work appears justified to identify improved SERS probe designs based on conventional fused-silica fibers.

This work was supported by the Australian Research Council under Discovery Project grant DP1092955. We would like to thank the RMIT Microscopy and Microanalysis Facility (RMIT University) for assistance with EDS measurements, Sasani Jayawardhana for helpful discussions, and Andrew Moore for technical assistance.

References

1. P. R. Stoddart and D. J. White, "Optical fibre SERS sensors," Anal. Bioanal. Chem **394**, 1761–1774 (2009).
2. R. A. Potyrailo, S. E. Hobbs, and G. M. Hieftje, "Optical waveguide sensors in analytical chemistry: today's instrumentation, applications and trends for future development," J. Am. Chem. Soc. **362**, 349–373 (1998).
3. Y. Han, M. K. K. Oo, Y. Zhu, L. Xiao, M. S. Demohan, W. Jin, and H. Du, "Index-guiding liquid-core photonic crystal fiber for solution measurement using normal and surface-enhanced Raman scattering," Opt. Eng. **47**, 040502 (2008).
4. H. Yan, C. Gu, C. Yang, J. Liu, G. Jin, J. Zhang, L. Hou, and Y. Yao, "Hollow core photonic crystal fiber surface-enhanced Raman probe," Appl. Phys. Lett. **89**, 204101 (2006).
5. Y. Zhang, C. Shi, C. Gu, L. Seballos, and J. Z. Zhang, "Liquid core photonic crystal fiber sensor based on surface enhanced Raman scattering," Appl. Phys. Lett. **90**, 193504 (2007).
6. M. K. K. Oo, Y. Han, J. Kanka, S. Sukhishvili, and H. Du, "Structure fits the purpose: photonic crystal fibers for evanescent-field surface-enhanced Raman spectroscopy," Opt. Lett. **35**, 466–468 (2010).
7. M. K. K. Oo, Y. Han, R. Martini, S. Sukhishvili, and H. Du, "Forward-propagating surface-enhanced Raman scattering and intensity distrubuition in photonic crystal fiber with immobilized Ag nanoparticles," Opt. Lett. **34**, 968–970 (2009).
8. C. Viets and W. Hill, "Comparison of fibre-optic SERS sensors with differently prepared tips," Sens. Acta B **51**, 92–99 (1998).
9. S. Jayawardhana, G. Kostovski, A. P. Mazzolini, and P. R. Stoddart, "Optical fiber sensor based on oblique angle deposition," Appl. Opt. **50**, 155–162 (2011).
10. Y. Komachi, H. Sato, K. Aizawa, and H. Tashiro, "Micro-optical fiber probe for use in an intravascular Raman endoscope," Appl. Opt. **44**, 4722–4732 (2005).
11. S. O. Konorov, C. J. Addison, H. G. Schulze, R. F. B. Turner, and M. W. Blades, "Hollow-core photonic crystal fiber-optic probes for Raman spectroscopy," Opt. Lett. **31**, 1911–1913 (2006).
12. S. Dochow, I. Latka, M. Becker, R. Spittel, J. Kobelke, K. Schuster, A. Graf, S. Brückner, S. Unger, M. Rothhardt, B. Dietzek, C. Krafft, and J. Popp, "Multicore fiber with integrated fiber Bragg gratings for background-free Raman sensing," Opt. Exp. **20**, 20156–20169 (2012).
13. J. Stadler, T. Schmid, and R. Zenobi, "Developments in and practical guidelines for tip-enhanced Raman spectroscopy," Nanoscale **4**, 1856–1870 (2012).
14. J. A. Dieringer, K. L. Wustholz, D. J. Masiello, J. P. Camden, S. L. Kleinman, G. C. Schatz, and R. P. van Duyne, "Surface-enhanced Raman excitation spectroscopy of a single rhodamine 6G molecule," J. Am. Chem. Soc. **131**, 849–854 (2009).
15. K. K. Maiti, U. S. Dinish, A. Samanta, M. Vendrell, K. Soh, S. Park, M. Olivo, and Y. Chang, "Multiplex targeted *in vivo* cancer detection using sensitive near-infrared SERS nanotags," Nano Today **7**(2), 85–93 (2012).
16. K. Ma, J. M. Yuen, N. C. Shah, J. T. Walsh, M. R. Glucksberg, and R. P. van Duyne, "*In vivo*, transcutaneous glucose sensing using surface-enhanced spatially offset Raman spectroscopy: multiple rats, improved hypoglycemic accuracy, low incident power, and continuous monitoring for greater than 17 days," J. Am. Chem. Soc. **83**, 9146–9152 (2011).
17. J. T. Motz, M. Hunter, L. H. Galindo, J. A. Gardecki, J. R. Kramer, R. R. Dasari, and M. S. Feld, "Optical fiber probe for biomedical Raman spectroscopy," Appl. Opt. **43**, 542–554 (2004).
18. S. Jayawardhana, A. P. Mazzolini, and P. R. Stoddart, "Collection efficiency of scattered light in single-ended optical fiber sensors," Opt. Lett. **37**, 2142–2144 (2012).
19. S. Jayawardhana, L. Rosa, S. Juodkazis, and P. R. Stoddart, "Additional enhancement of electric field in surface-enhanced Raman scattering due to Fresnel mechanism," Sci. Rep. **3**, 2335 (2013).
20. J. Ma and Y. Li, "Fiber Raman background study and its application in setting up optical fiber Raman probes," Appl. Opt. **35**, 2527–2533 (1996).
21. H. Sato, H. Shinzawa, and Y. Komachi, "Fiber-optic Raman probes for biomedical and pharmaceutical applications," in *Emerging Raman Applications and Techniques in Biomedical and Pharmaceutical Fields*, P. Matousek and M. D. Morris, eds. (Springer, 2010), pp. 25–45.
22. G. Keiser, *Optical Fiber Communications* (McGraw-Hill, 2000).
23. R. Buividas, P. R. Stoddart, and S. Juodkazis, "Laser fabricated ripple substrates for surface-enhanced Raman scattering," Ann. Phys. **524**, L5–L10 (2012).
24. G. Kostovski, U. Chinnasamy, S. Jayawardhana, P. R. Stoddart, and A. Mitchell, "Sub-15 nm optical fiber nanoimprint lithography: a parallel, self-aligned and portable approach," Adv. Mater **23**, 531–535 (2011).
25. J. D. Caldwell, O. Glembocki, F. J. Bezares, N. D. Bassim, R. W. Rendell, M. Feygelson, M. Ukaegbu, R. Kasica, L. Shirey, and C. Hosten, "Plasmonic nanopillar arrays for large-area, high-enhancement surface-enhanced Raman scattering sensors," ACS Nano **5**, 4046–4055 (2011).
26. A. Polemi, S. M. Wells, N. V. Lavrik, M. J. Sepaniak, and K. L. Shuford, "Local field enhancement of pillar nanosurfaces for SERS," J. Phys. Chem. C **114**, 18096–18102 (2010).
27. F. L. Galeener, "The Raman spectra of defects in neutron bombarded and Ge-rich vitreous GeO_2," J. Non-Cryst. Solids **40**, 527–533 (1980).
28. R. Scarmozzino, A. Gopinath, R. Pregla, and S. Helfert, "Numerical techniques for modeling guided wave photonic devices," IEEE J. Sel. Top. Quantum Electron. **6**, 150–162 (2000).
29. D. J. White and P. R. Stoddart, "Nanostructured optical fiber with surface-enhanced Raman scattering functionality," Opt. Lett. **30**, 598–600 (2005).